Journal of Molecular Catalysis A: Chemical 340 (2011) 15–23

Contents lists available at ScienceDirect

Journal of Molecular Catalysis A: Chemical

journal homepage: www.elsevier.com/locate/molcata

Editor's choice paper

Decomposition of ethanol over Ni/Al_2O_3 catalysts to produce hydrogen and carbon nanostructured materials

Daniela Zambelli Mezalira[a,b], Luiz Dias Probst[a], Stéphane Pronier[b], Yann Batonneau[b], Catherine Batiot-Dupeyrat[b,*]

[a] Departamento de Química, Universidade Federal de Santa Catarina, CP 476, 88040-900 Florianópolis, Brazil
[b] Laboratoire de Catalyse en Chimie Organique, ESIP, UMR-CNRS 6503, 40 avenue du Recteur Pineau, 86022 Poitiers Cedex, France

ARTICLE INFO

Article history:
Received 12 October 2010
Received in revised form 9 March 2011
Accepted 16 March 2011
Available online 31 March 2011

Keywords:
Ethanol
Catalytic decomposition
Supported nickel catalysts
Hydrogen production
Carbon nanostructure

ABSTRACT

γ-Alumina-supported 10, 20 and 33 wt.% nickel catalysts were prepared and used to investigate the decomposition of ethanol to hydrogen and carbon materials at 500 and 700 °C. It was verified that the ethanol conversion was complete for all nickel loadings at 500 and 700 °C. A low nickel loading (10 and 20%) favored the formation of the very stable spinel phase $NiAl_2O_4$, which has low activity in the production of solid carbon. The maximum hydrogen and carbon production was obtained using a nickel loading of 33%: more than 6 g of solid carbon per gram of catalyst (gC/g_{cat}) was produced at 700 °C and 22.2 gC/g_{cat} when the reaction was performed at 500 °C. At 500 °C, nanofibers were mainly formed, while at 700 °C the production of multiwalled nanotubes was favored. The selectivity in terms of the gaseous products was dependent on the nickel loading and temperature used. At high temperature the partial thermal decomposition of ethanol was favored leading, mainly, to the production of hydrogen, methane, and carbon monoxide. At 500 °C, there was the production of ethylene on the Al_2O_3 surface with low nickel loading. With high nickel loading (33%) ethanol decomposition to hydrogen and nanostructured carbon was favored

1. Introduction

Hydrogen production is of great industrial interest since hydrogen is considered to be an ideal fuel for fuel cells. Hydrogen is mainly produced by steam reforming of natural gas and more recently also by decomposition of methane. The latter has the advantage of generating carbon nanostructured materials (carbon nanofibers and nanotubes) [1–3].

Carbon nanotubes (CNTs) and carbon nanofibres (CNFs) offer many extraordinary physical and chemical properties, for instance, they can be used as supports for metal catalysts [4] and to strengthen composite materials [5]. CNTs can be produced by three technologies: carbon-arc discharge, laser-ablation and catalytic decomposition processes. The latter method has been reported to be the most selective toward carbon nanotube formation; arc discharge and laser-ablation leading to mixtures of carbon materials. Transition metals, such as nickel, iron and cobalt, are the most commonly used catalysts for the growth of filamentous carbon [6–8]. The source of carbon is hydrocarbons, mainly methane, from natural gas.

In order to make the processes more environmental friendly the use of ethanol, easily produced from biomass, has been developed to produce hydrogen by steam reforming [9,10]. The use of ethanol as a carbon source for the synthesis of CNTs was first reported by Maruyama et al. [11].

More recently, Li et al. [12,13] have reported an interest in using ethanol to produce hydrogen and CNTs simultaneously. The authors showed that Fe/Al_2O_3 and Co/C catalysts were quite active in the production of CNTs and hydrogen.

Wang et al. [14] studied the catalytic performance of Ni/Al_2O_3 catalyst prepared by a hydrothermal method for the decomposition of ethanol to produce hydrogen and CNTs. The authors focused on the effect of Ni loadings and reaction temperature on the production of H_2 and CNTs. They showed that the hydrogen production increased with increasing temperature (from 500 to 800 °C) while the quantity and quality of nanotubes decreased due to the sintering of Ni particles.

In this study we propose an extensive investigation of the catalytic decomposition of ethanol using Ni/Al_2O_3 catalyst prepared by a wet impregnation method. We focus on the composition of the gas phase in order to determine what are the main reactions involved in the process at two different temperatures: 500 and 700 °C. The effect of nickel loading and calcinations temperature were investigated. The influence of the catalyst composition on the simultaneous production of hydrogen and MWCNTs is discussed.

* Corresponding author. Tel.: +33 05 49 45 38 98; fax: +33 05 49 45 33 49.
E-mail address: catherine.batiot.dupeyrat@univ-poitiers.fr (C. Batiot-Dupeyrat).

1381-1169/$ – see front matter © 2011 Elsevier B.V. All rights reserved.
doi:10.1016/j.molcata.2011.03.013

2. Experimental part

2.1. Catalyst preparation

Ni catalysts were prepared by the wet impregnation method, using nickel nitrate [$Ni(NO_3)_2{\cdot}6H_2O$] (Sigma–Aldrich) as the metal precursor. Known amounts of the nickel salt (to obtain a metal content of 10, 20, and 30%) were dissolved in water and commercial aluminum oxide [γ-Al_2O_3] (AL-3996R, Engelhard Exceptional Technologies) was added under continuous stirring. The slurries thus obtained were heated slowly to 90 °C and maintained at that temperature until nearly all the water had evaporated. The solid residues were dried at 100 °C for 24 h and then calcined in air at 700 °C for 5 h. The catalyst with 30 wt.% of nickel was calcined at 300, 500 and 700 °C, for 5 h.

2.2. Characterization of catalyst and reaction products

Catalyst samples were characterized using N_2 physisorption isotherms (Micromeritics TriStar - Surface and Porosity Analyzer). Specific surface areas were calculated according to the Brunauer–Emmett–Teller (BET) method. Prior to the measurements, the samples were outgassed at 350 °C for 8 h.

Nickel loading was measured using a Perkin Elmer (Optima 2000 DV) inductively coupled plasma-optical emission spectrometer (ICP-OES) after the catalyst calcinations.

The catalysts were characterized by X-Ray Diffraction (XRD) using a Siemens D-5005 diffractometer with CuKα = 1.5417 Å, operated at 40 kV and 30 mA. The diffraction patterns were recorded in the 2θ range of 10–90° with a step interval of 0.02° and period of 1 s.

Temperature Programmed Reduction (TPR) analysis was carried out with a Micromeritics Autochem 2910 analyzer using approximately 100 mg of catalyst. These experiments were performed using a 5% H_2/Ar flow and the temperature was raised at 5 °C min^{-1} from room temperature to 900 °C and maintained at this temperature for 30 min.

Transmission Electron Microscopy (TEM) images were obtained on a Philips CM120 instrument equipped with a LaB_6 filament. The sample was deposited on a Cu grid for observation by TEM. The diameters of carbon nanotubes were evaluated from about 20 images and 100 measurements.

Thermogravimetric analysis (TGA) was carried out with a SDT 2960 thermobalance TA Instruments analyzer in Pt crucibles to determine the stability of the carbon formed. The measurement of several samples was performed under an airflow of 100 cm^3 h^{-1} on heating from room temperature to approximately 700 °C with a heating rate of 5 °C min^{-1}.

Raman spectra (Stokes spectra) were obtained at room temperature, using an HR UV 800 confocal scanning spectrometer (Horiba Jobin Yvon) equipped with a Peltier-cooled charge-coupled device (1152 × 298 pixels) for detection. The Raman scattering was excited using a 632.81 nm excitation wavelength supplied by an internal He–Ne laser through an Olympus high-stability BXFM confocal microscope. Patterns were recorded in the 50–1000 cm^{-1} Raman shift range with a spectral resolution of 0.5 cm^{-1}. LabSPEC v. 5 software was used for data acquisition and processing.

2.3. Catalytic reaction

Catalytic decomposition of ethanol was carried out at atmospheric pressure, in a horizontal fixed-bed reactor at a temperature of either 500 or 700 °C. Prior to this step, the catalyst was reduced *in situ* using a 15% H_2/N_2 flow at 700 °C for 30 min. Ethanol was pumped into a tubular furnace (0.04 mL min^{-1}) and vaporized. The gaseous ethanol was then mixed with nitrogen (volumetric mixture ratio of ethanol/nitrogen = 1/1). A total flow rate of 40 mL min^{-1} was then fed to the reactor containing 100 mg of the catalyst. Effluents released by the reactor were analyzed using a gas chromatograph (Perkin-Elmer) equipped with a Flame Ionization Detector (FID) and Thermal Conductivity Detector (TCD). Separations were performed using a carboxen 1000 column for CO and CO_2, a Poraplot Q column for CH_4, C_2H_6 and C_2H_4, and a molecular sieve 5A column for H_2. Reaction data were recorded for 4 h. Catalyst activity was evaluated in terms of ethanol conversion. We defined ethanol conversion as:

$$\text{Ethanol conversion}(\%) = \frac{\text{mol ethanol in} - \text{mol ethanol out}}{\text{mol ethanol out}} \times 100$$

The molar concentration of products was calculated using a standard mixture. The calculation is expressed as follows:

$$\text{Molar concentration of products}(\%) = \frac{ni}{n\ \text{total}} \times 100$$

where *ni* is the moles of *i* gas product (H_2, CH_4, CO, CO_2, C_2H_4, C_2H_6), *n* total is the total moles of gas (N_2, H_2, CH_4, CO, CO_2, C_2H_4, C_2H_6).

Table 1
Catalyst active phase loading and specific surface area before and after calcination at 700 °C.

Catalysts	Ni (wt.%) ICP-OES	S_{BET} (m^2 g^{-1})	
		Before reduction	After reduction
10 wt.% Ni/Al_2O_3	9.8	162	156
20 wt.% Ni/Al_2O_3	20.4	104	102
30 wt.% Ni/Al_2O_3	33.3	116	100

3. Results and discussion

3.1. Characterization of the catalyst before reaction: nickel loading and influence of the calcination temperature

The nickel loadings of the catalysts as determined by ICP-OES are reported in Table 1. It can be observed that the amount of nickel for the catalysts with 10 and 20 wt.% is close to the target value, while the third catalyst is composed of 33% nickel. To simplify the notation the samples were designated as 10NiAL, 20NiAl and 33NiAl.

The specific surface areas of the catalysts calcined at 700 °C are also indicated in Table 1, and the values exceeded 100 m^2 g^{-1} for all nickel loadings.

With the aim of identifying the phases present in the catalytic samples, X-ray diffraction and TPR analysis were carried out. After the drying step, samples of the catalyst 33NiAl were calcined at 300, 500 and 700 °C under air for 5 h. Fig. 1 shows the XRD profiles. Broad peaks indicate that the Al_2O_3 phase is weakly crystallized. In the presence of nickel, as the calcination temperature increases the formation of the spinel $NiAl_2O_4$ occurs. It is difficult to identify precisely the diffraction lines of $NiAl_2O_4$ due to overlap with those of the γ-Al_2O_3 phase and some diffraction lines of NiO. Nevertheless, the presence of $NiAl_2O_4$ when the calcination temperature exceeds 500 °C is well documented in the literature [15]. The presence of NiO can be evidenced by the diffraction peak at 2θ = 63° corresponding to the NiO (2 2 0) plane. When the calcination temperature increases the peaks become more intense and narrower, indicating an increase in the average NiO crystallite size [16].

Fig. 2 shows the XRD patterns obtained for the 10NiAl, 20NiAl and 33NiAl samples after calcination at 700 °C. Broad peaks were obtained with lower nickel loadings (10 and 20%) and the peaks were narrower for the highest nickel loading indicating the presence of larger NiO crystallites.

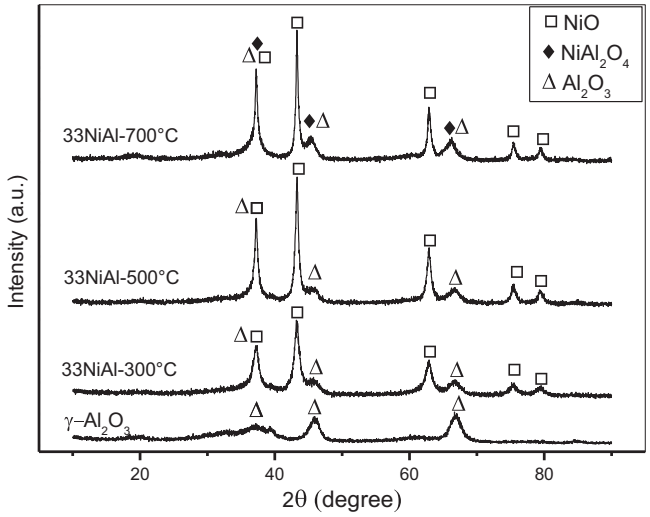

Fig. 1. XRD patterns obtained over 33 wt.% Ni/γ-Al_2O_3 calcined at different temperatures (300, 500 and 700 °C).

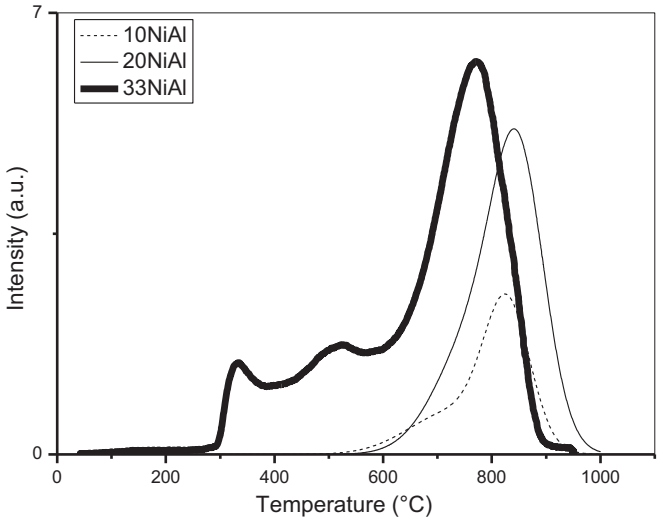

Fig. 3. H_2-TPR profiles obtained over Ni/γ-Al_2O_3 calcined at 700 °C with different amounts of Ni loading (10, 20 and 33%).

The TPR profiles for the 10NiAl, 20NiAl and 33NiAl samples after calcination at 700 °C are displayed in Fig. 3. We checked that the hydrogen consumption during the H_2-TPR corresponds to a complete reduction of nickel in the temperature range: 300–1000 °C.

The TPR profiles of the samples with low nickel loading (10NiAl and 20NiAl) showed the presence of a large peak between 600 and 1000 °C. This peak was attributed to the reduction of stoichiometric nickel aluminate ($NiAl_2O_4$) [17,18]. The 10NiAl sample clearly showed a shoulder at close to 700 °C indicating the presence of nonstoichiometric nickel aluminate (NiO–Al_2O_3) [19]. This shoulder did not appear in the case of the 20NiAl sample, perhaps because the $NiAl_2O_4$ phase, which overlaps with the NiO–Al_2O_3 phase, was present in greater quantity. For the 33NiAl catalyst three main peaks are clearly visible. In the lowest temperature region (300–400 °C) the peak corresponds to the bulk NiO, with some interaction with the support. The second peak (400–600 °C) indicates a stronger interaction between NiO and Al_2O_3, while the third (600–900 °C) is attributed to the presence of the nickel aluminate.

The diffusion of nickel and/or aluminum from one phase to the other is probably dependent on the nickel loading. The driving force for the diffusion of nickel and/or aluminum is likely to be the concentration gradient between the nickel oxide and the aluminum oxide phases [20]. From the H_2-TPR results it can be concluded that the diffusion of nickel ions into the Al_2O_3 is not complete with 33 wt.% of nickel, this amount corresponding to the quantity of Ni in $NiAl_2O_4$.

Consequently, it is proposed that, after calcination at 700 °C, the catalyst composition is as follows, depending on the nickel content:

$$10\%Ni/Al_2O_3\text{: } Al_2O_3 + NiAl_2O_4(10NiAl)$$

$$20\%Ni/Al_2O_3\text{: } Al_2O_3 + NiAl_2O_4(20NiAl)$$

$$33\%Ni/Al_2O_3\text{: NiO} + Al_2O_3 + NiAl_2O_4(33NiAl)$$

The influence of the calcination temperature for 33NiAl is reported in Fig. 4. The samples calcined at 300 and 500 °C are easily reduced compared to that calcined at 700 °C. The H_2 consumption observed before 300 °C indicates the presence of nickel nitrate used as the metal precursor and this is not completely eliminated during the calcination step. We can observe that the samples calcined

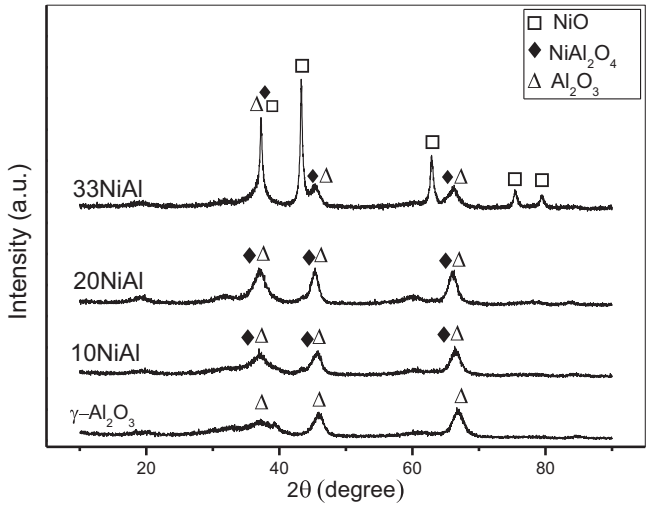

Fig. 2. XRD patterns obtained over Ni/γ-Al_2O_3 calcined at 700 °C with different amounts of Ni loading (10, 20 and 33%).

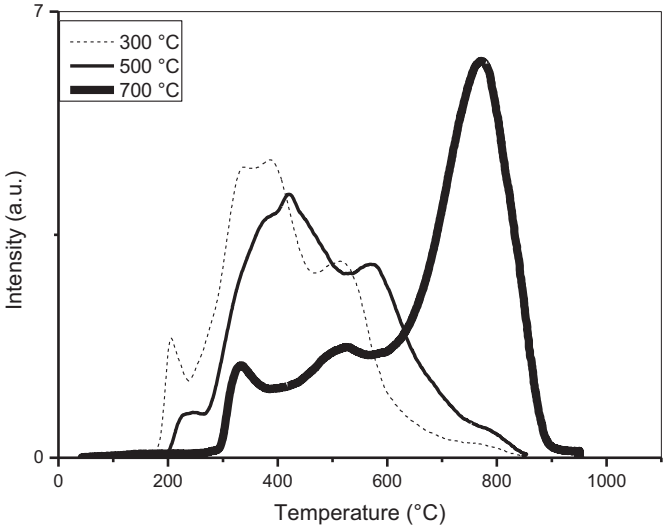

Fig. 4. H_2-TPR profiles obtained over 33 wt.% Ni/γ-Al_2O_3 calcined at different temperatures.

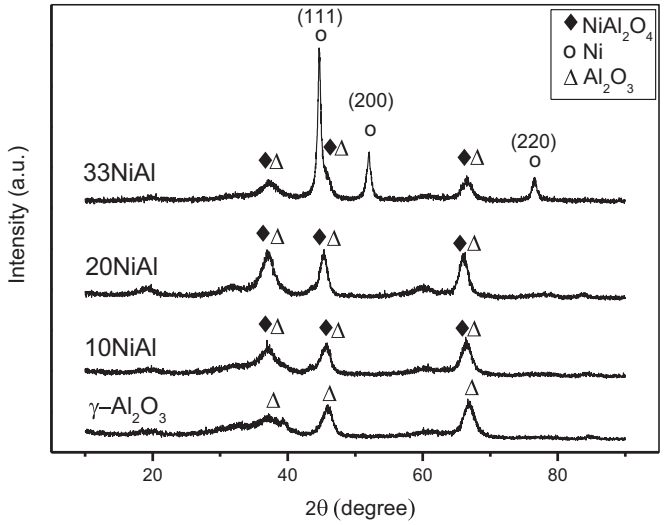

Fig. 5. XRD patterns obtained after reduction at 700 °C of Ni/γ-Al_2O_3 with different amounts of Ni loading (10, 20 and 33%).

at 300 and 500 °C have only a very small reduction peak at 800 °C, indicating that the preponderant phase is NiO and not $NiAl_2O_4$. Generally, low temperature peaks are attributed to the reduction of NiO particles presenting a weak interaction with the support, while the higher temperature peaks are attributed to the reduction of NiO and strong interaction with the oxide support.

The H_2-TPR not only allows the catalyst behavior to be investigated under a reductive atmosphere, it is also an interesting tool to verify the nature of the oxide phases obtained, complementing the data obtained from the XRD analysis.

3.2. Characterization of the catalyst after reduction

The catalysts calcined at 700 °C were reduced under hydrogen at 700 °C for 30 min prior to the reactions. As shown in Table 1 the surface area is not significantly modified by the reduction step regardless of the nickel loading. Only a small decreased was observed, values remaining higher than 100 $m^2 g^{-1}$. The surface area of the starting alumina support was equal to 200 $m^2 g^{-1}$, consequently the nickel impregnation followed by the calcination at 700 °C leads to a slight decrease of the surface area of the material.

The XRD measurements performed after the reduction step are reported in Fig. 5. After the treatment under hydrogen at 700 °C, the XRD patterns obtained with the 10NiAl and 20NiAl samples were not significantly different from the patterns obtained before the reduction (presence of both Al_2O_3 and $NiAl_2O_4$). These results are explained by the stability of the spinel phase $NiAl_2O_4$ towards reduction, as a temperature of 700 °C is not sufficient to reduce completely $NiAl_2O_4$.

For the catalyst 33NiAl, the presence of metallic nickel particles is clearly evidenced from the XRD pattern, indicating that the catalyst was reduced at 700 °C. The presence of the spinel phase $NiAl_2O_4$ cannot be established, from XRD, due to the overlapping of the $NiAl_2O_4$ diffraction lines with the γ-Al_2O_3 phase. However according to the H_2-TPR profile, the presence of $NiAl_2O_4$ after the reduction step at 700 °C, can be proposed.

The 33NiAl catalyst showed peaks at $2\theta = 44°$, 51° and 76° corresponding to three nickel planes (1 1 1), (2 0 0) and (2 2 0), respectively. The nickel crystallite size was calculated for the 33NiAl sample using the Ni (1 1 1) reflection and the Debye–Scherrer equation. The calculated crystallite sizes were found to be 13 nm after the reduction step verifying that relatively small nickel particles are present. The presence of such small nickel particles is also visible in the TEM images as shown in Fig. 6. It can be explained by the low amount of metallic nickel particles at the surface of the support compared to the high concentration of nickel in the bulk. However, the presence of some nickel particles of close to 20 nm are also visible, which can be attributed to the large amount of nickel used [14].

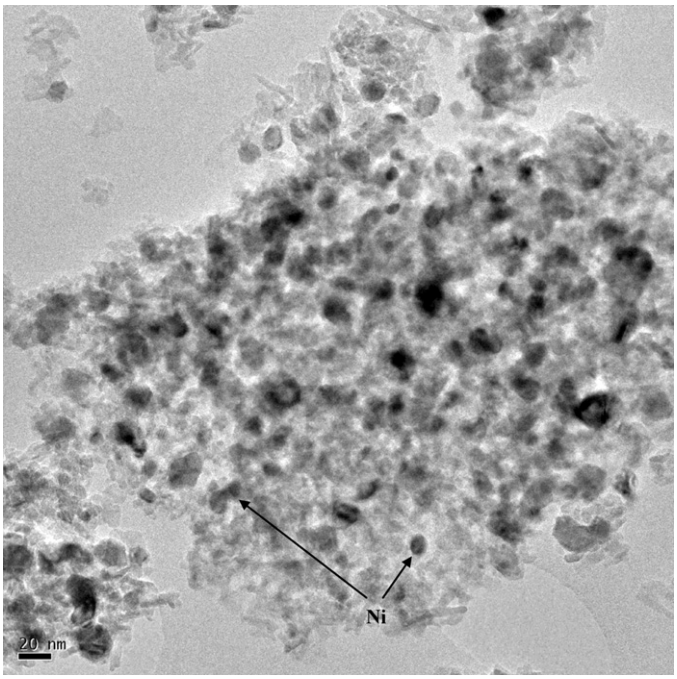

Fig. 6. TEM micrograph after reduction of 33 wt.% Ni/γ-Al_2O_3 under hydrogen at 700 °C.

3.3. Catalytic reaction

In order to investigate the catalytic activity of the different Ni/Al_2O_3 catalysts, the decomposition of ethanol was carried out. The catalytic decomposition of ethanol was performed at two different temperatures, at 500 and 700 °C. Prior to this study the thermal decomposition of ethanol was investigated at temperatures from 200 to 700 °C (Fig. 7). The results showed that ethanol decomposition is not significant at 500 °C and is complete at 700 °C.

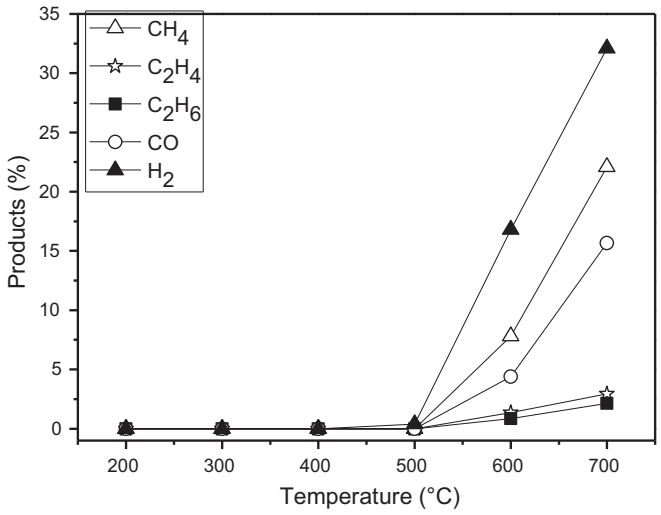

Fig. 7. Thermal decomposition of ethanol from 200 to 700 °C.

Table 2
Influence of the nickel loading on the catalytic decomposition of ethanol.

Catalyst	Reaction T (°C)	Reaction time (min)	% Products						C prod (g/g_{cat})
			H_2	CO	CO_2	CH_4	C_2H_4	C_2H_6	
10NiAl	700	30	27.0	13.0	0.6	14.1	3.0	2.5	
	700	240	20.4	13.4	0.4	21.8	2.2	2.4	0.33
	500	30	14.0	0.5	2.0	0.2	30.5	0.3	
	500	240	18.6	0.5	4.1	0.2	30.3	0.2	1.16
20NiAl	700	30	29.0	12.0	0.7	13.1	2.4	2.4	
	700	240	22.5	13.1	0.5	20.8	2.1	2.3	1.02
	500	30	20.5	0.5	4.0	0.9	26.0	0.6	
	500	240	20.8	0.7	4.5	0.4	30.5	0.4	2.99
33NiAl	700	30	31.5	12.2	1.0	10.8	0	0	
	700	240	23.5	13.5	0.8	19.1	1.9	2.2	6.35
	500	30	29.5	1.5	3.5	17.5	0.2	0	
	500	240	30.2	1.1	4.5	14.0	4.3	0.3	22.2

Table 3
Ethanol transformation with 33 wt.% Ni/γ-Al_2O_3 at 500 °C based on carbon balance.

C_2H_5OH	C	CH_4	CO_2	C_2H_4	C_2H_6	CO
100%	54%	24%	10%	9%	1%	2%

From the GC analysis, it is possible to ascertain the composition of the exhaust gases at 700 °C: hydrogen (33%), methane (23%), carbon monoxide (15%), ethylene and ethane (3%). The presence of water was indicated, but it was not possible to quantify.

The results show that hydrogen can be produced simply through the thermal treatment of ethanol; however, the presence of undesired products, such as methane, in high yields makes this process of using ethanol to produce hydrogen unviable.

The influence of the presence of the nickel-based catalysts is shown in Table 2. The catalysts with different nickel loading were calcined at 700 °C. In all cases total conversion of ethanol was achieved.

The carbon production is calculated with the formula:

$$C_{\text{production}}(g/g_{\text{cat}}) = \frac{(m_T - m_{\text{cat}})}{m_{\text{cat}}}$$

where m_T is the total mass of catalyst and carbon produced after 4 h of reaction, m_{cat} is the mass of catalyst used (100 mg).

Table 2 shows that the production of carbon is low for 10NiAl and 20NiAl at all reaction temperatures; however, the production of carbon reaches 22.2 gram per gram of catalyst with 33NiAl at 500 °C. For all samples, as the reaction temperature increases from 500 to 700 °C the amount of carbon produced decreases, which can be attributed to two different scenarios:

(1) The nature of the carbon materials produced. Indeed at 500 °C, carbon nanofibers (CNFs) are mainly formed (see below) while carbon nanotubes (CNTs) are produced at 700 °C. The higher density of CNFs compared to CNTs can explain the higher yield in weight of carbon obtained at low temperature.
(2) A partial thermal decomposition of ethanol. When the reaction is performed at 700 °C, not only the catalyst bed is heated at 700 °C but also the gas mixture (ethanol and nitrogen), before entering the catalyst zone. Consequently, it is to be expected that ethanol is partially decomposed into CO, C_2H_6 and C_2H_4. The presence of such products, which are not as easily activated by the catalyst as ethanol, could explain the lower yield of carbon at 700 °C.

Table 4
Ethanol transformation with 30 wt.% Ni/γ-Al_2O_3 at 500 °C based on hydrogen balance.

C_2H_5OH	H_2	CH_4	H_2O	C_2H_4	C_2H_6
100%	42%	32%	19%	6%	1%

The effect of temperature on the activity of Ni/Al_2O_3 catalyst has been largely studied in the literature. Alberton et al. [21] studied the influence of temperature on the carbon formation during ethanol steam reforming over Ni/Al_2O_3 catalysts. The authors showed that the deactivation of the catalyst was lower at 973 K than at 773 K while the amount of deposited carbon was slightly higher. They explained their results by the formation of encapsulating carbon during the initial stages of the reaction at 773 K, while filamentous carbon is preferably formed at 973 K. In our experimental conditions the formation of encapsulating carbon can be envisaged at 773 K, nevertheless the ethanol conversion remains 100%, showing that ethanol is still activated at 773 K even after 75 h of reaction. Moreover, the difference in the morphology of carbon material is evidenced by the TEM images, the lowest reaction temperature (500 °C) favoring the production of dense carbon material (carbon nanofibers) compared to the highest reaction temperature (700 °C) showing the presence of carbon nanotubes.

Jeong and Lee [7] investigated the growth of filamentous carbon by decomposition of ethanol on nickel foam. They showed that the most favorable temperature was around 600 °C: only a thin layer of carbon covers the nickel foam at 550 °C and the foam surface is clean at 750 °C. The authors explained the results by the role of the Boudouard reaction ($2CO = C + CO_2$) favored at relatively low temperature.

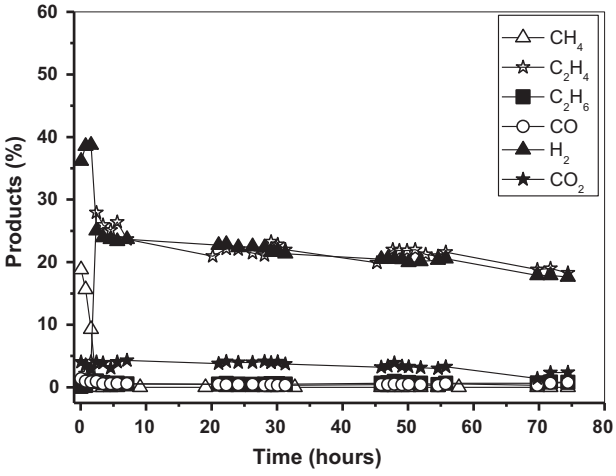

Fig. 8. Long term experiment with 33NiAl at 500 °C.

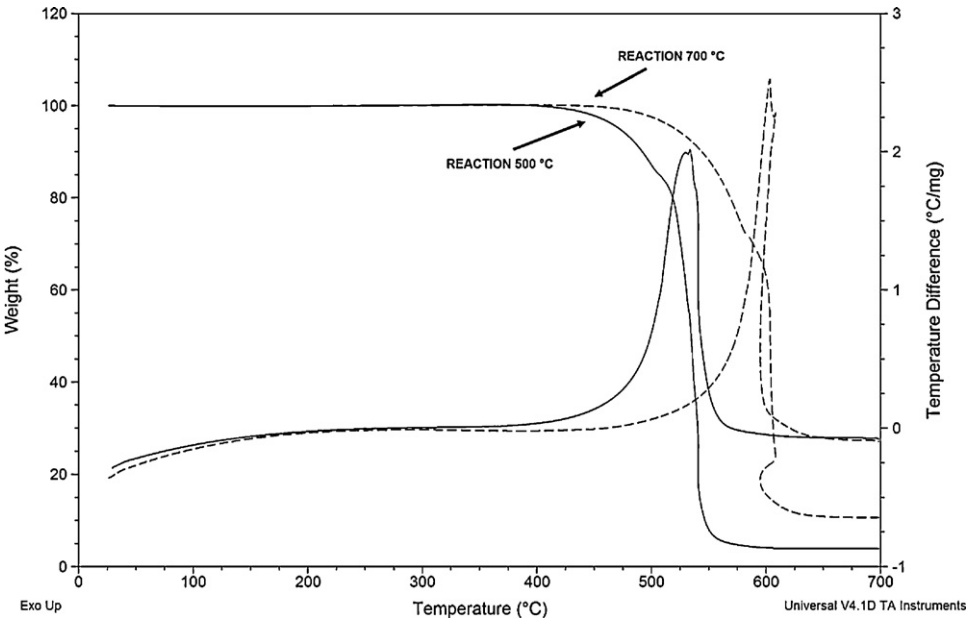

Fig. 9. TGA of the sample after 4 h of reaction at 500 and 700 °C with 33 wt.% Ni/γ-Al_2O_3.

So we can see that the influence of the temperature for the reactivity of ethanol over nickel based catalysts can be explained by considering the reactions involved or by the mechanism of carbon deposition. It seems difficult to conclude at this stage; most probably the two phenomenons are combined.

According to the gas phase composition and the thermodynamic data, the main reactions involved in the catalytic decomposition of ethanol can be proposed as follows:

$$CH_3CH_2OH \rightarrow CO + H_2 + CH_4 \quad (1)$$

$$CH_3CH_2OH \rightarrow CH_2{=}CH_2 + H_2O \quad (2)$$

Subsequent reactions can proceed from the products, such as:

$$CH_4 \rightarrow C + 2H_2 \quad (3)$$

$$C_2H_4 \rightarrow 2C + 2H_2 \quad (4)$$

Ethylene can be hydrogenized as follows:

$$CH_2{=}CH_2 + H_2 \rightarrow CH_3{-}CH_3 \quad (5)$$

The gas phase composition with 10NiAl and 20NiAl could be explained as follows:

- At 500 °C, the dehydration of ethanol to ethylene is favored ($\Delta G^\circ = -52.9$ kJ/mol), the direct cracking of ethylene to carbon can proceed at this low temperature whereas methane cracking is not favored at 500 °C ($\Delta G^\circ = 5$ kJ/mol). Consequently, the resulting carbon formation can be attributed to ethylene decomposition. Indeed, the amount of CO and CH_4 is very low which shows that reaction (1) is not favored. These results show that the mixture of Al_2O_3 and spinel $NiAl_2O_4$ favors the dehydration of ethanol. The dehydration properties of Al_2O_3 have been evidenced by Rosynek et al. [22] and Fatsikostas et al. [23].
- At 700 °C, the thermal decomposition of ethanol according to reaction (1) is favored but the dehydration of ethanol can also proceed. The carbon deposition would result from methane or ethylene decomposition. This hypothesis is corroborated by the composition of the exhaust gas, which is similar to the composition obtained without a catalyst.

The catalyst 33NiAl is much more active than 10NiAl and 20NiAl due to the presence of metallic nickel on the support after the reduction step. The maximum hydrogen production and a particularly high carbon yield are obtained with 33NiAl.

The very low ethylene production with 33NiAl can be explained by the ethanol activation on metallic nickel particles at the surface of the support (after the reduction step) which is responsible for bond cleavage to produce mainly hydrogen and carbon.

At 500 °C, methane is present most probably due to ethylene cracking at the surface of nickel particles or to reaction (1) followed by CO methanation. The methanation of CO being favored in the presence of metallic nickel particles and low temperature, it is thus not possible to exclude the methanation of CO as a possible reaction. At 700 °C with 33NiAl, the product distribution is not very different from those obtained using 10NiAl and 20NiAl proving that a thermal effect can be mainly responsible of the gas phase composition. However the amount of carbon deposition is much higher with 33NiAl than with 10NiAl and 20NiAl, so the direct decomposition of ethanol or ethylene decomposition is strongly favored at the surface of nickel metal.

In addition, according to the TPR and XRD results, the $NiAl_2O_4$ phase formation is greater for these samples, indicating a greater metal–support interaction. Thus, the active phase (Ni) is expected to be less accessible and the support mainly responsible for the catalytic activity.

A modification of the selectivity toward CH_4 and H_2 can be noted over time on stream when the reaction is performed at 700 °C, the selectivity toward methane increases while at the same time the selectivity toward hydrogen decreases regardless of the nature of the catalyst. This result can be attributed to the formation of carbon which is not highly structured (such as amorphous carbon) and which can react with hydrogen to produce methane.

The amount of carbon dioxide produced is very low for all of the catalysts and reaction temperatures investigated. The presence of CO_2 can result from steam reforming of ethanol:

$$C_2H_5OH + 3H_2O \rightarrow 6H_2 + 2CO_2 \quad \Delta G(500\,^\circ C) = -125\ \text{kJ mol}^{-1} \quad (6)$$

Based on the gas phase composition, the above-mentioned reactions, and the carbon and hydrogen balance, it is possible to estimate the ethanol transformation. The results reported in

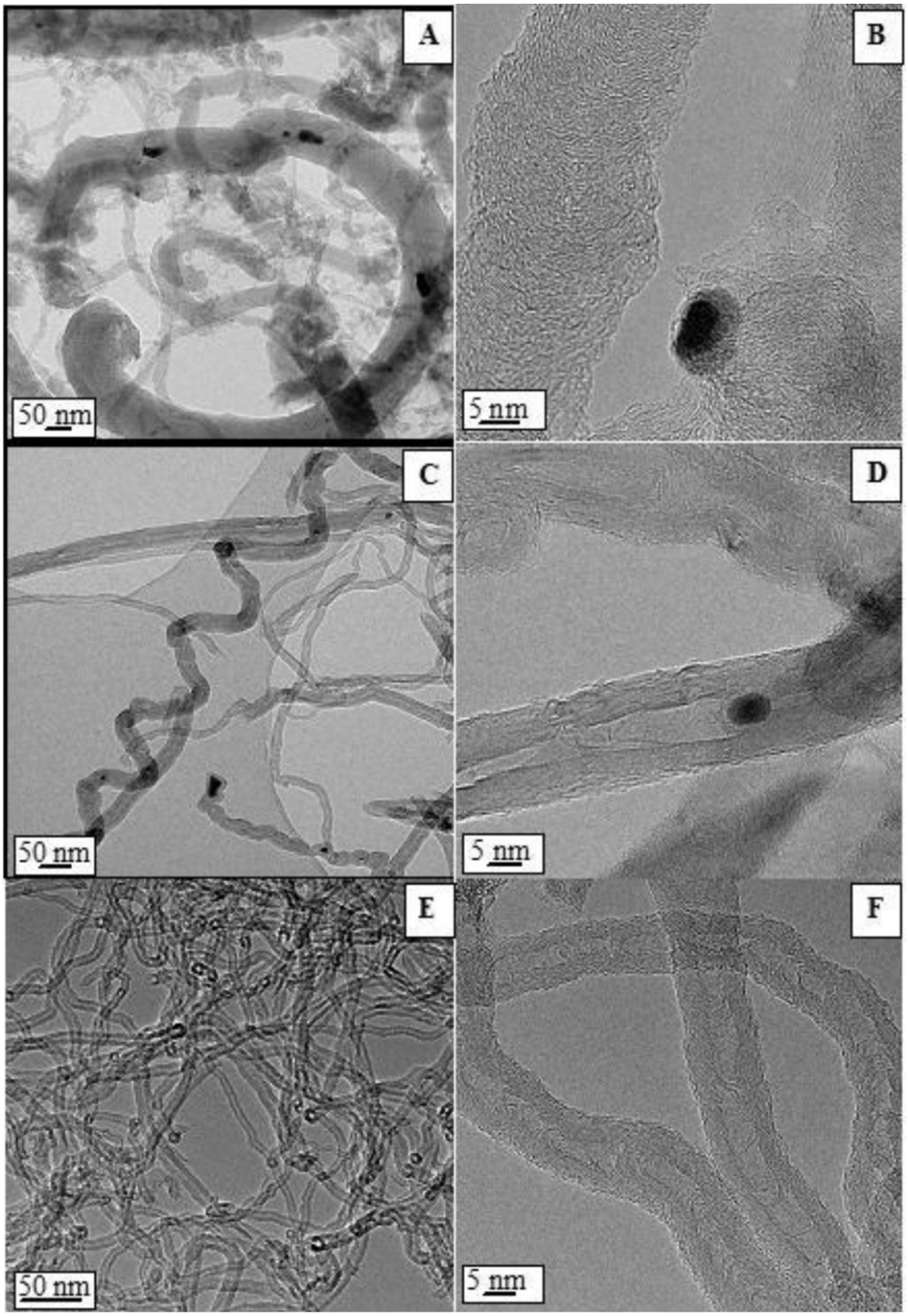

Fig. 10. TEM images of carbon formed after 4 h of reaction over: 33 wt.% Ni/γ-Al_2O_3 at 500 °C (A and B) and 700 °C (C and D), over 10 wt.% Ni/γ-Al_2O_3 at 700 °C (E and F).

Tables 3 and 4 were obtained with the catalyst 33NiAl at 500 °C: 55% of the carbon present in the ethanol is transformed into carbon deposits, 24% into methane, 10% into carbon dioxide, 9% into ethylene, 2% into carbon monoxide, and 1% into ethane (Table 3). From the hydrogen balance (Table 4), it is clear that a high amount of the hydrogen present in the ethanol is converted into methane (32%), while 42% is converted into hydrogen, 19% into water, 6% into ethylene and 1% into ethane.

A long term experiment was performed using the 33NiAl catalyst at 500 °C. The reaction was carried out using a flow of ethanol of 0.05 mL/min, with the appropriate flow of nitrogen to obtain a ratio of $C_2H_5OH/N_2 = 1$. Fig. 8 shows that the hydrogen production is high during the first five hours of reaction and then sharply decreases from 35% to 25%. At the same time the production of methane decreases, which shows that the ethanol decomposition according to reaction 3 is less favorable after 5 h of reaction. The production of carbon monoxide is always low even at the beginning of the reaction, indicating that CO reacts to generate carbon according to the following reactions:

$$2CO \rightarrow C + CO_2 (\Delta G^{\circ}_{500\,^{\circ}C} = -35.27\,kJ\,mol^{-1}) \quad (7)$$

$$CO + H_2 \rightarrow C + H_2O (\Delta G^{\circ}_{500\,^{\circ}C} = -24.91\,kJ\,mol^{-1}) \quad (8)$$

$$CO + 3H_2 \rightarrow CH_4 + H_2O (\Delta G^{\circ}_{500\,^{\circ}C} = -30.02\,kJ\,mol^{-1}) \quad (9)$$

The deactivation of the catalyst can be explained by a change in the accessibility of the nickel particles. At the beginning of the reaction metallic nickel particles are available for the activation of ethanol and its decomposition to hydrogen, methane and carbon monoxide, but when the amount of solid carbon produced becomes high, nickel particles are covered by or encapsulated in the carbon nanotube/nanofiber (see Fig. 10). Consequently, the activation of C_2H_5OH is limited and its dehydrogenation at the surface of the support (mainly $NiAl_2O_4$) is favored. This is corroborated by the presence of ethylene in high yields after a few hours of reaction. However, the growth of the carbon fibers continues for 75 h on stream, the amount of solid carbon reaching 31 g/g_{cat}.

3.4. Characterization of the carbon produced

Thermogravimetric analysis (TGA) was performed after 4 h of reaction at 500 °C and 700 °C over 33NiAl. Fig. 9 shows that no amorphous carbon, easily oxidized at around 320 °C, is present in the samples. The mass-loss step occurs at 450–550 °C when the reaction is performed at 500 °C, and at 550–620 °C for the reaction at 700 °C, accounting for the higher stability of the carbon formed at higher temperatures. The TGA curve has a shoulder immediately before the sharp weight loss. This shoulder could be attributed to the presence of filled filaments at 500 °C and thick multiwalled carbon nanotubes at 700 °C.

The TEM images in Fig. 10(A and B) shows that carbon fibers are present after the reaction at 500 °C with the catalyst 33NiAl, heterogeneous filaments are formed with external diameters of between 7 and 150 nm and internal diameters of 1.5–3 nm. When the reaction is conducted at 700 °C, multiwalled carbon nanotubes with external diameters of 8–50 nm and internal diameters of 4–12 nm are formed. The presence of carbon nanofibers has also been evidenced by Chen et al. [16] for the same type of catalyst at 500 °C during methane decomposition. It is generally accepted that carbon growth takes place on the nickel particle according to a dissolution–precipitation mechanism [24]. The greater thickness of the walls formed at 500 °C may be attributed to the easier solubility of carbon in the nickel particles at low temperature [25]. Fig. 10(E and F) shows that carbon nanotubes are also formed at 700 °C with the catalyst 10NiAl. It proves that 10NiAl is partly reduced to form metallic nickel during the step under hydrogen at 700 °C. However the amount of CNTs obtained is low: 0.33 g/g_{cat} which results from the low amount of reduced nickel available for the growth of CNTs. This result is in accordance with the H_2-TPR profile showing that the reduction of the spinel phase $NiAl_2O_4$ starts at 600 °C but is complete after 950 °C.

Raman spectroscopy was used to characterize the nanotubes. The spectra exhibit similar features (Fig. 11). Two intense peaks are observed at 1323–1325 cm^{-1} and 1575–1581 cm^{-1} which are assigned to the D and G peaks, respectively. The D peak is disorder-induced and thus indicative of disordered carbon, multiwalled tubes and microcrystalline graphite. The G peak is the only peak originating from a normal first-order Raman scattering process of E_{2g} symmetry and results from the tangential stretching mode of graphitic-like materials. In addition, the D′ peak [26] typical of disordered graphite is detected as a shoulder in all the samples. Spectral features were fitted to Lorentzian curves, from which the relative intensities of the D and G bands were determined.

The I_D/I_G ratio is known to be dependent on the size of the graphitic crystallites. The lower this ratio the higher the degree of crystallinity and the lower the defects in the sidewalls of nanotubes [27,28]. The I_D/I_G values are very similar for all amounts of nickel present in the catalyst (Fig. 10). It seems that this parameter does not affect significantly the quality of the nanotubes. However, the higher I_D/I_G value obtained for 33 wt.% Ni/γ-Al_2O_3 when the reaction was performed at 700 °C could indicate a slight increase in the disorder and decrease in the size (diameter) of the carbon material when compared with the reaction carried out at 500 °C in presence of the same catalyst with a constant ethanol flow rate of 0.04 mL min^{-1}.

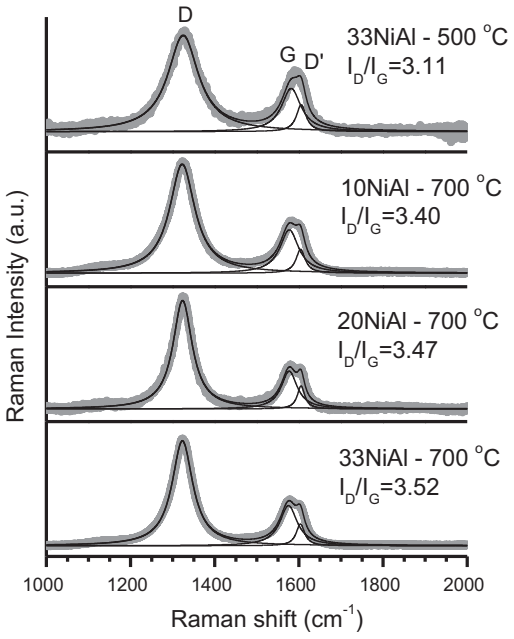

Fig. 11. Raman spectra of nanotubes obtained over 30% Ni/γ-Al_2O_3 calcined at 700 °C after 4 h of reaction at 500 °C and over Ni/γ-Al_2O_3 calcined at 700 °C with different amounts of Ni loading (10, 20 and 30%) after 4 h of reaction at 700 °C. Experimental data are represented in grey, band components and the sum of the components by solid lines.

4. Conclusions

The decomposition of ethanol over Ni/γ-Al_2O_3 catalysts with different nickel loadings (10, 20 and 33%) was investigated at two different temperatures: 500 and 700 °C. The production of carbon materials is low with 10 and 20% nickel loading, which can be attributed to the formation of the very stable spinel phase $NiAl_2O_4$ during the calcination step at 700 °C. TPR experiments revealed that the reduction of $NiAl_2O_4$ requires temperatures higher than 900 °C. Consequently, metallic nickel species are not available to perform the decomposition of ethanol over the 10 and 20% Ni/Al_2O_3 materials. When the nickel loading reaches 33%, the presence of nickel oxide is evidenced by XRD after calcination. The reduction of 33NiAl at 700 °C leads to the formation of metallic nickel particles responsible for the high catalytic activity and more than 6 g of solid carbon per gram of catalyst is produced at 700 °C, this reaching 22.2 gC/g_{cat} when the reaction is performed at 500 °C. The characterization of carbon formed after 4 h of reaction shows that carbon fibers are produced at 500 °C while multiwalled carbon nanotubes are produced at 700 °C.

The conversion of ethanol is complete at 500 °C and 700 °C for all nickel loadings. When the reaction is performed at 700 °C it is assumed that a partial thermal decomposition of ethanol occurs which produces not only hydrogen but also methane and carbon monoxide in high yields.

At 500 °C, 10NiAl and 20NiAl catalysts promote the formation of ethylene due to the dehydrogenation properties of Al_2O_3 while with 33NiAl the CO_2 production is very low and the decomposition of ethanol proceeds readily to produce hydrogen and solid carbon.

Thus, according to the results presented here, the optimum experimental conditions are obtained at 500 °C using a 33% nickel loading over alumina.

Acknowledgement

The authors are grateful to the Brazilian research funding, CNPq, for the financial support.

References

[1] R.M. Almeida, H.V. Fajardo, D.Z. Mezalira, G.B. Nuernberg, L.K. Noda, L.F.D. Probst, N.L.V. Carreno, J. Mol. Catal. 259 (2006) 328–335.
[2] A. Venugopal, S.N. Kumar, J. Ashok, D.H. Prasad, V.D. Kumari, K.B.S. Prasad, M. Subrahmanyam, Int. J. Hydrogen Energy 32 (2007) 1782–1788.
[3] G.B. Nuernberg, H.V. Fajardo, D.Z. Mezalira, T.J. Casarin, L.F.D. Probst, N.L.V. Carreño, Fuel 87 (2008) 1698–1704.
[4] J.M. Planeix, N. Coustel, B. Coq, V. Brotons, P.S. Kumbhar, R. Dutartre, P. Geneste, P. Bernier, P.M. Ajayan, J. Am. Chem. Soc. 116 (1994) 7935–7936.
[5] M.M.J. Treacy, T.W. Ebbesen, J.M. Gibson, Nature 381 (1996) 678–680.
[6] M. Pérez-Cabero, I. Rodríguez-Ramos, A. Guerrero-Ruíz, J. Catal. 215 (2003) 305–316.
[7] N. Jeong, J. Lee, J. Catal. 260 (2008) 217–226.
[8] S. Noda, H. Sugime, T. Osawa, Y. Tsuji, S. Chiashi, Y. Murakami, S. Maruyama, Carbon 44 (2006) 1414–1419.
[9] M. Virginie, M. Araque, A.C. Roger, J.C. Vargas, A. Kiennemann, Catal. Today 138 (2008) 21–27.
[10] M.A. Goula, S.K. Kontou, P.E. Tsiakaras, Appl. Catal. B 49 (2004) 135.
[11] S. Maruyama, R. Kojima, Y. Miyauchi, S. Chiashi, M. Kohno, Chem. Phys. Lett. 360 (2002) 229.
[12] W. Li, H. Wang, Z. Ren, G. Wang, J. Bai, Appl. Catal. B: Environ. 84 (2008) 433–439.
[13] J. Diao, H. Wang, W. Li, G. Wanga, Z. Ren, J. Bai, Physica E 42 (2010) 2280–2284.
[14] G. Wang, H. Wang, Z. Tang, W. Li, J. Bai, Appl. Catal. B: Environ. 88 (2009) 142–151.
[15] Z. Xu, Y. Li, J. Zhang, L. Chang, R. Zhou, Z. Duan, Appl. Catal. A: Gen. 210 (2001) 45–53.
[16] J. Chen, Q. Ma, T.E. Rufford, Y. Li, Z. Zhu, Appl. Catal. A: Gen. 362 (2009) 1–7.
[17] X.L. Zhu, P.P. Huo, Y.P. Zhang, D.G. Cheng, Appl. Catal. B: Environ. 81 (2008) 132.
[18] G. Wen, Y. Xu, Z. Xu, Z. Tian, Catal. Lett. 129 (2009) 250–257.
[19] T.A. Maia, J.D.A. Bellido, E.M. Assaf, J.M. Assaf, Quim. Nova 30 (2007) 339–345.
[20] B. Vos, E. Poels, A. Bliek, J. Catal. 198 (2001) 77–88.
[21] A.L. Alberton, M.V.M. Souza, M. Schmal, Catal. Today 123 (2007) 257–264.
[22] M.P. Rosynek, R.J. Koprowski, G.N. Dellisante, J. Catal. 122 (1990) 80–94.
[23] A.N. Fatsikostas, X.E. Verykios, J. Catal. 225 (2004) 439–452.
[24] J. Rostrup-Nielsen, D.L. Trimm, J. Catal. 48 (1977) 155–165.
[25] M. Inoue, K. Asai, Y. Nagayasu, K. Takane, S. Iwamoto, E. Yagasaki, K.-I. Ishii, Diamond Relat. Mater. 17 (2008) 1471–1475.
[26] M.S. Dresselhaus, G. Dresselhaus, in: M. Cardona, G. Güntherodt (Eds.), Light Scattering in Solids, vol. III, Springer, Berlin, 1982, pp. 3–58.
[27] F. Tuinstra, J.L. Koenig, J. Chem. Phys. 53 (1970) 1126.
[28] K. Nakamura, M. Fujitsuka, M. Kitajima, Phys. Rev. B 41 (1990) 12260.